Trilayer multiorbital models of $La_4Ni_3O_{10}$

Cui-Qun Chen, Zhihui Luo,[*] Meng Wang, Wéi Wú, and Dao-Xin Yao[†]
Center for Neutron Science and Technology, Guangdong Provincial Key Laboratory of Magnetoelectric Physics and Devices, State Key Laboratory of Optoelectronic Materials and Technologies, School of Physics, Sun Yat-Sen University, Guangzhou 510275, China

(Received 10 February 2024; revised 3 June 2024; accepted 20 June 2024; published 2 July 2024)

Recently, the discovery of superconductivity in Ruddlesden-Popper (RP) $La_4Ni_3O_{10}$ under pressure has further expanded the realm of nickelate-based superconductor family. In this paper, we perform a first-principles study of $La_4Ni_3O_{10}$ for both the $P2_1/a$ phase at ambient pressure and $I4/mmm$ phase at high pressure, with $U = 0$, 3.5 eV. Our results confirm the characteristic upward shift of a Ni-d_{z^2} bonding band under pressure. Moreover, our analysis of electronic spectrum and orbital occupancy unveil the dynamic mechanism of electronic reconstructions under pressure, embedded in a critical dual effect. Based on our results, we further propose a trilayer two-orbital model by performing Wannier downfolding on Ni-e_g orbitals. Our model reveals four Fermi surface sheets with α, β, β', γ pockets, bearing resemblance to that of bilayer $La_3Ni_2O_7$. According to the model, our calculated spin susceptibility under random phase approximation shows that the $d_{x^2-y^2}$ orbital is also important for the magnetic fluctuation in the RP series. Finally, a high energy 16-orbital model with direct dp, pp hoppings is proposed, which implies that $La_4Ni_3O_{10}$ also lies in the charge-transfer picture within the Zaanen-Sawatzky-Allen scheme. Our exposition of electronic reconstructions and multiorbital models shed light on theoretical electronic correlation study and experimental exploration of lower pressure superconductors in the RP series.

DOI: 10.1103/PhysRevB.110.014503

I. INTRODUCTION

The recently consecutive discoveries of nickelate-based superconductors from infinite-layer nickelates RNiO$_2$ ($R =$ La,Nd,Pr) [1–3] to Ruddlesden-Popper (RP) series nickelates $La_{n+1}Ni_nO_{3n+1}$ ($n = 2, 3$) [4–10], have drawn intensive investigations in the field of high-T_c superconductivity [11–44], particularly in the aspect of how correlations renormalize the low-lying electronic states and potentially drive the unconventional pairing in these compounds [26–40,42]. Also, for RNiO$_2$, the sample-dependent factors, such as defects, impurity, and domains deserve careful consideration [2,45]. For RP series nickelates, pressure is undoubtedly in the center of the road map, as the observations of zero resistance always correlate with a structure transition, and further promote the electronic reconstructions [4,7,9–11,46]. The reconstructions exhibit a quite general trend among this series, which is largely manifested in the upward shift of Ni-d_{z^2} states towards Fermi energy [4,11,47]. It is widely believed that such an upward shift should be responsible for the emergence of superconductivity. However, there still lacks comprehension of the dynamic mechanism of these reconstructions, which is indeed fundamental and indispensable. Furthermore, inspections of layer dependence is another important aspect. These are crucial to unveiling superconducting mechanisms in the RP series.

In bilayer $La_3Ni_2O_7$, the structure at ambient pressure is characterized by octahedral-distorted $Amam$ (space group 63), which transits to octahedral-regular $Fmmm$ phase (space group 69) roughly in the range of $10 \sim 15$ GPa [5,6,8] within orthorhombic lattice. Surprisingly, this range highly coincides with the full development of superconducting T_c from 0 to 80 K [4–6]. For pressure up to $\sim$19 GPa, a higher symmetric $I4/mmm$ (space group 139) phase within tetragonal lattice is emergent [48,49], where T_c exhibits a certain amount of decrease [4–6]. In trilayer $La_4Ni_3O_{10}$, an analogous monoclinic $P2_1/a$ (space group 14) phase is characterized at ambient pressure, which transits to the $I4/mmm$ phase roughly in the range of $12 \sim 15$ GPa. However, the maximal T_c merely reaches $20 \sim 30$ K under a much higher pressure of about 43 GPa [7]. These further suggest some critical roles of pressure to be clear in the series.

In this paper, we perform a comprehensive first-principles study of trilayer $La_4Ni_3O_{10}$ for both $P2_1/a$ phase at ambient pressure (AP) and $I4/mmm$ phase at high pressure (HP). Our resulting electronic structure and microscopic multiorbital models strongly suggest an alike superconducting mechanism as compared with $La_3Ni_2O_7$. Moreover, based on our DFT results, we clarify the dynamic mechanism of such electronic reconstructures, which is of importance for a comprehensive understanding of superconductivity in the RP series.

The paper is organized as follows. In Sec. II, we first analyze the structure difference of the $P2_1/a$ phase at AP and $I4/mmm$ phase at HP, which can provide readers a general understanding of the pressure effect on the lattice level. On this basis, in Sec. III, we present the detailed settings of

[*]Contact author: luozhh28@mail2.sysu.edu.cn
[†]Contact author: yaodaox@mail.sysu.edu.cn

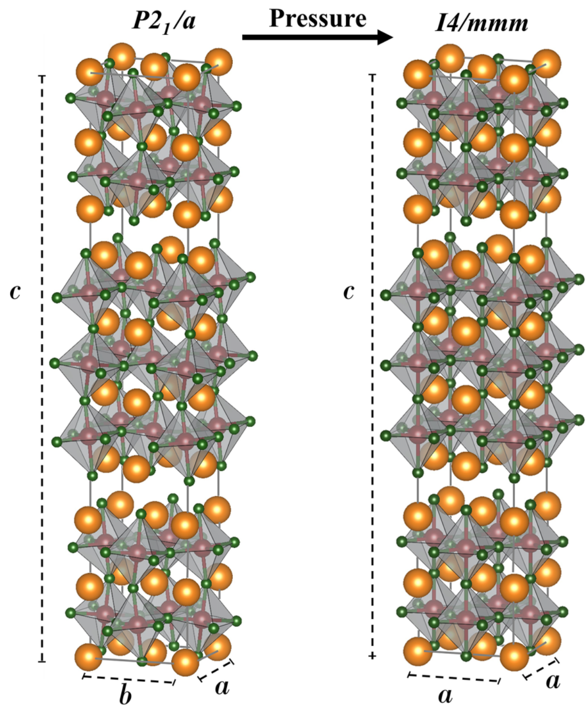

FIG. 1. Structure of the trilayer nickelate $La_4Ni_3O_{10}$ for both $P2_1/a$ and $I4/mmm$ phases. The red, green, and orange balls represent the nickel, oxygen, and lanthanum atoms, respectively. The grey area shapes the Ni-O octahedra. a, b, c denote the lattice constants.

our DFT calculations. In Sec. IV A, we present our main DFT results, which include band structures and electronic spectra for both phases, with $U = 0$, 3.5 eV. The charge transfer processes and valence under pressure are also particularly analyzed in this section. In Sec. IV B, we establish an effective trilayer two-orbital model based on our DFT results. In Sec. IV C, we investigate the spin susceptibility based on the model. In Sec. IV D, we further propose a high energy 16-orbital model. In Sec. V, we provide discussions regarding the dynamic mechanism of electronic reconstructions and layer dependence, followed by the summary in Sec. VI.

II. STRUCTURE TRANSITION UNDER PRESSURE

In trilayer $La_4Ni_3O_{10}$, each Ni ion is surrounded by six oxygen sites forming NiO_6 octahedron. The corner-shared stacking of these octahedrons gives rise to NiO_2 trilayers, as well as the important interlayer Ni-O-Ni bond along c axis. Both structures of the AP $P2_1/a$ and HP $I4/mmm$ phases are demonstrated in Fig. 1. The schematic reveals two major differences: (1) For the AP phase, there are perceivable octahedral tiltings as compared with the HP phase. (2) Also, both phases are differentiated in the lattice constants under a $\sqrt{2} \times \sqrt{2}$ lattice, in which the AP phase shows orthorhombic distortion with unequal a, b lengths, while the HP phase possesses square structure. According to Ref. [47], the lattice constants are $a = 5.4675$, $b = 5.4164$, $c = 27.9564$ Å for AP, and $a = 5.1769$, $c = 26.2766$ Å for HP at 44.3 GPa, which corresponds to 15% of the lattice collapse. It should be noted that there are also several other types of structure distortions in the RP series, such as octahedral rotation and bond disproportionation of NiO_6 octahedron. But their implications on electronic structure are quite insignificant compared with octahedral tilting [49]. In fact, for $La_4Ni_3O_{10}$, there exists another phase of *Bmab* (space group 64) at AP which survives in high temperature. This phase differs from $P2_1/a$ phase by a relative octahedral rotation, while both band structures are almost indistinguishable around E_F [50].

III. METHOD DETAILS

Density functional theory (DFT) calculations were performed with VIENNA AB INITIO SIMULATION PACKAGE (VASP) [51,52], in which the projector augmented wave [53,54] method within the framework of the local density approximation (LDA) [55] exchange correlation potential is applied. The energy cutoff of the plane-wave expansion was set as 600 eV and a Γ-centered $20 \times 20 \times 19$ Monkhorst Pack k-mesh grid was adopted. In structural relaxations, we adopted the experimental refined lattice constants for both phases [47], which is the $P2_1/a$ phase at ambient pressure and the $I4/mmm$ phase at pressure of 44.3 GPa. The convergence criterion of force was set to 0.001 eV/Å and total energy convergence criterion was set to 10^{-7}eV. In band-structure calculations, we adopted a $\sqrt{2} \times \sqrt{2}$ primitive cell for the $I4/mmm$ phase to have a direct comparison with $P2_1/a$ phase, as both contain six Ni atoms. To obtain the projected tight-binding models, we further performed Wannier downfolding as implemented by WANNIER90 [56] package, in which the good convergences were reached.

IV. RESULTS

The DFT results are carefully examined, which are in agreement with previous theoretical calculations [47,50] as well as the reported ARPES results [57]. On this basis, we adopted a very large k-mesh size as mentioned before to determine the precise Fermi level, which is important given the flat band feature in this material.

A. Electronic structure

In Fig. 2, we present the electronic structures of $La_4Ni_3O_{10}$ for both AP $P2_1/a$ and HP $I4/mmm$ phases. Here the upper and lower panels represent the cases of $U = 0$ and 3.5 eV, respectively. From these band structures, we can observe the dominant Ni-d_{z^2} (blue) and $d_{x^2-y^2}$ (red) orbitals around Fermi energy, which is quite similar to the bilayer system [4,11,58]. For the Ni-d_{z^2} band, it clearly exhibits the characteristic three-branch structure, which corresponds to bonding, nonbonding, and antibonding states with increasing energy, as indicated in Fig. 2(a) [47,59]. Apart from the Ni-e_g sector, there also appear dense bands (grey) away from E_F, which can be found in the density of states (DOS) [Figs. 2(c) and 2(f)] associating with the Ni-t_{2g} sector around −1 eV (orange) and the La sector around 3 eV (cyan).

Next, we discuss the electronic reconstructions under pressure. As expected, that pressure is prone to enhance the itinerancy of electrons, which in our case corresponds to a ratio of ∼1.3 to the increase of bandwidth from AP to HP, as illustrated in Figs. 2(a) and 2(b) for $U = 0$ eV and

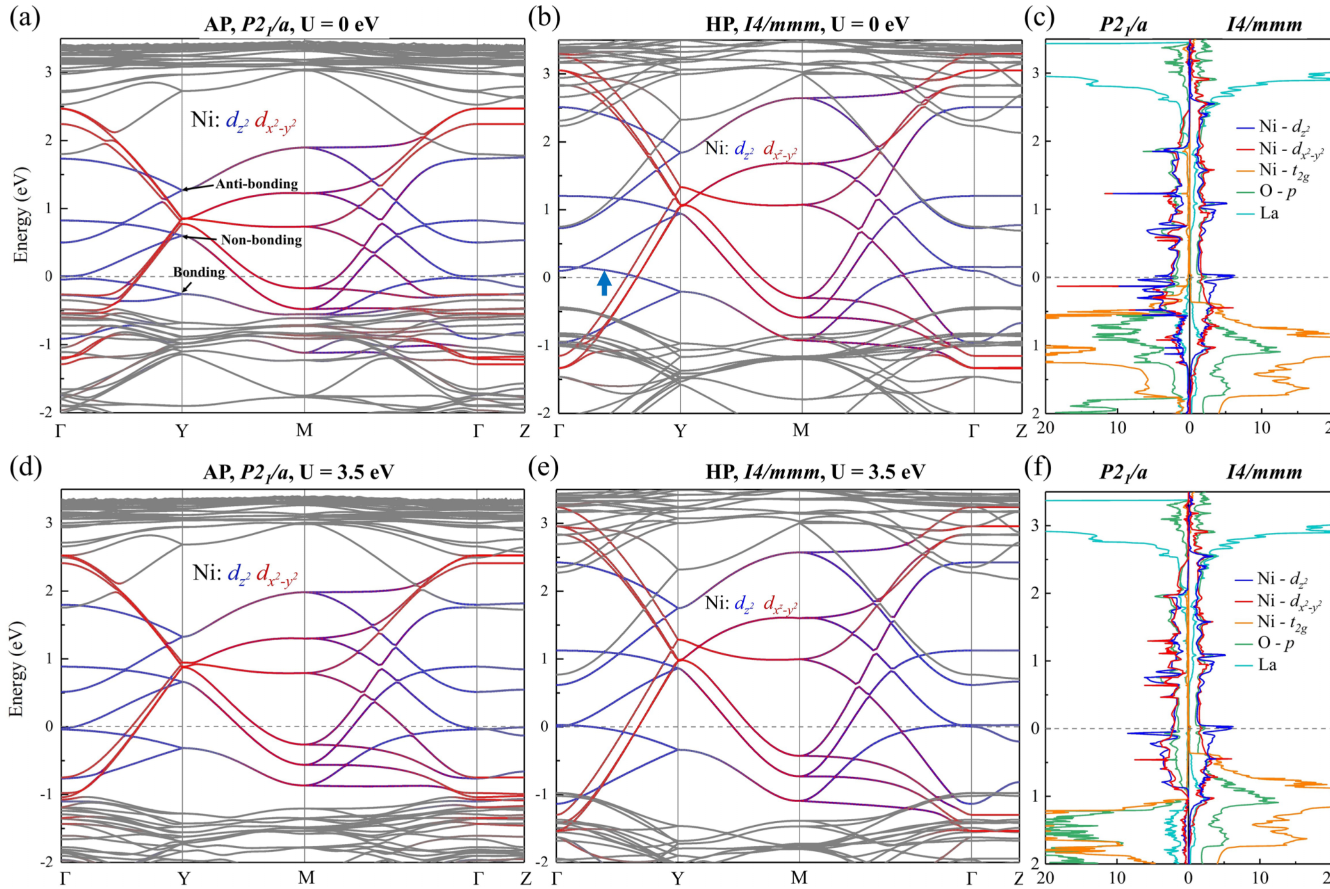

FIG. 2. Electronic structure of $La_4Ni_3O_{10}$. DFT (LDA) calculated band structures of $La_4Ni_3O_{10}$ at $U = 0$ eV (a), (b) and $U = 3.5$ eV (d), (e) for AP $P2_1/a$ phase and HP $I4/mmm$ phase. The blue and red colors are spectral weights for d_{3z^2} and $d_{x^2-y^2}$ orbitals, respectively. (c), (f) Projected DOS of $La_4Ni_3O_{10}$ at AP (left panel) and HP (right panel). The blue, red, orange, green, and cyan colors denote the projection of Ni-$d_{3z^2-r^2}$, Ni-$d_{x^2-y^2}$, Ni-t_{2g}, O-p, and La orbitals.

Figs. 2(d) and 2(e) for $U = 3.5$ eV. As we further zoom in to the Fermi level, for AP phase (left panel), we observe a very narrow gap relating the bonding and nonbonding bands at the Γ point [47,50]. Forthe HP phase (middle panel), the bonding band gets upward shifted as a hole pocket for both $U = 0$, 3.5 eV. It is worth noting that, for $U = 3.5$ eV [Fig. 2(e)], such a hole pocket is almost flat right at E_F, giving rise to a sharp peak in DOS, further highlighting a crucial link to the superconductivity [60,61] in the RP series.

Given such a critical band upward shift under pressure, we further address the corresponding charge transfer process. In Table I, we present the orbital occupancies of Ni-d, O-p orbitals for both phases at $U = 0$ eV. It is clear that both e_g orbitals are over half filling at AP, while pressure tends to depress their occupancies, and become almost half filling at HP. We noted that the decrease of $n^{\mathrm{Ni}}_{x^2-y^2}$ is hardly identified in band structure, although it has a relatively smaller amount than that of $n^{\mathrm{Ni}}_{z^2}$. But for the t_{2g} sector, pressure has an opposite effect, in which $n^{\mathrm{Ni}}_{t_{2g}}$ is increased from about 5.9 to 6, i.e., fully filled at HP. Such a trend can also be observed in Figs. 2(c) and 2(f), in which the t_{2g} spectrum is closer to E_F for AP phase. Also, for oxygen occupancies, we find their variations are quite insignificant under pressure. Finally, the table reveals a slight charge imbalance between the inner and outer layers, and we find that these trends and magnitudes are quite close to that of DFT + DMFT results at HP [62]. This highlights that our results at $U = 0$ eV are also valid for the consideration of correlation effect.

In view of the above analysis, we can quantitatively obtain some crucial charge transfer magnitudes from AP to HP based

TABLE I. DFT calculated ($U = 0$ eV) orbital occupancies of $La_4Ni_3O_{10}$ for both the AP $P2_1/a$ phase and HP $I4/mmm$ phase. Here $n^{\mathrm{O}}_{p_x/p_y}$ denotes one of the in-plane O-p_x, p_y orbitals that is elongated along its adjacent Ni site. For $n^{\mathrm{O}}_{p_z}$, the rows of inner and outer denote the apical O-p_z orbitals that are inside and outside the trilayer, respectively. Note that for the AP phase, each value is averaged appropriately over doubled atoms.

	Layer	$n^{\mathrm{Ni}}_{x^2-y^2}$	$n^{\mathrm{Ni}}_{z^2}$	$n^{\mathrm{Ni}}_{t_{2g}}$	$n^{\mathrm{O}}_{p_x/p_y}$	$n^{\mathrm{O}}_{p_z}$
AP	Inner	1.199	1.289	5.874	1.695	1.656
	Outer	1.173	1.241	5.942	1.698	1.861
HP	Inner	1.066	1.022	5.996	1.675	1.641
	Outer	1.077	1.100	5.993	1.696	1.843

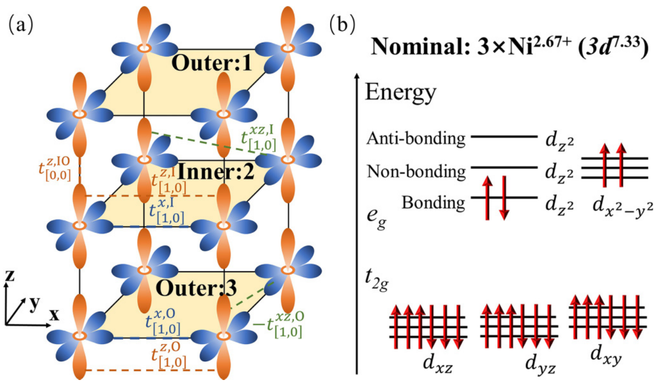

FIG. 3. (a) Schematic of trilayer $La_4Ni_3O_{10}$ lattice. The blue and orange shapes denote Ni-d_{z^2} and $d_{x^2-y^2}$ orbitals, respectively. Some of the hoppings of the trilayer two-orbital model are drawn, whose values can be found in Table II; also see text for details. (b) Electronic configuration of $La_4Ni_3O_{10}$. The arrows indicate nominal configuration $3d^{7.33}$.

on Table I. Overall, there is an average $3d^{8.36} \rightarrow 3d^{8.14}$ for Ni ions. Specifically, $2.44 \rightarrow 2.14$ for Ni-e_g and $5.92 \rightarrow 6.0$ for Ni-t_{2g} sectors. However, for oxygen ions, an average $\sim$1.7 valence is persistent. Here, if we assume full ionization of oxygens, we would alternatively obtain an average $d^{7.36} \rightarrow d^{7.14}$, in which the former value is quite close to the nominal $d^{7.33}$ configuration. These charge transfers imply a critical dual effect of pressure on microscopic electronic structures. On one hand, pressure promotes a charge redistribution within Ni-3d orbitals, which can alter the relative renormalization effects of these orbitals. In particular, the involvement of the t_{2g} sector near E_F could enhance the charge fluctuation at AP, which is relevant to the observed charge density wave [7,63]. On the other hand, the electric neutrality indicates a pressure-driven charge transfer from Ni to La ions (the transfer to Ni-4s orbitals is negligible). In fact, from Figs. 2(a) and 2(b), we can also see a notable drop of the lowest La band from about 2 to 0.7 eV at Γ point, which implies a general downward shift of the La spectrum. This feature further indicates an enhanced $d-f$ hybridization at HP above E_F, especially with the Ni-d_{z^2} orbital, which might be observed in resonant inelastic x-ray scattering signal [64].

B. Trilayer two-orbital model

To gain more insights into the electronic property that is directly relevant to the superconductivity, in the following sections, we focus on the HP $I4/mmm$ phase. Based on the DFT electronic structure, we further perform Wannier downfolding on the trilayer Ni-e_g orbitals at $U = 0$ eV, which allows us to build an effective trilayer two-orbital model:

$$\mathcal{H} = \mathcal{H}_t + \mathcal{H}_U, \quad \mathcal{H}_t = \sum_{\mathrm{k}\sigma} \Psi^\dagger_{\mathrm{k}\sigma} H(\mathrm{k}) \Psi_{\mathrm{k}\sigma},$$

$$\begin{aligned}\mathcal{H}_U &= U \sum_{i}^{\alpha=1,2,3} \left(n^{x_\alpha}_{i\uparrow} n^{x_\alpha}_{i\downarrow} + n^{z_\alpha}_{i\uparrow} n^{z_\alpha}_{i\downarrow}\right) \\ &\quad + U' \sum_{i\sigma}^{\alpha=1,2,3} n^{x_\alpha}_{i\sigma} n^{z_\alpha}_{i\bar{\sigma}} + (U' - J_H) \sum_{i\sigma}^{\alpha=1,2,3} n^{x_\alpha}_{i\sigma} n^{z_\alpha}_{i\sigma} \\ &\quad + J_H \sum_{i}^{\alpha=1,2,3} \big(d^\dagger_{ix_\alpha\uparrow} d^\dagger_{ix_\alpha\downarrow} d_{iz_\alpha\downarrow} d_{iz_\alpha\uparrow} \\ &\quad - d^\dagger_{ix_\alpha\uparrow} d_{ix_\alpha\downarrow} d^\dagger_{iz_\alpha\downarrow} d_{iz_\alpha\uparrow} + \mathrm{H.c.}\big). \end{aligned} \tag{1}$$

The model $\mathcal{H}$ is composed of the tight-binding $\mathcal{H}_t$ and Coulomb interaction $\mathcal{H}_U$. The basis is $\Psi_\sigma = (d_{x_1\sigma}, d_{x_2\sigma}, d_{x_3\sigma}, d_{z_1\sigma}, d_{z_2\sigma}, d_{z_3\sigma})^T$, in which $d_{x_\alpha\sigma}$ denotes annihilation of a $d_{x^2-y^2}$ electron in the αth layer with spin σ, etc. The notation of layer is demonstrated in Fig. 3(a). For $\mathcal{H}_U$, there have four terms in full Kanamori form [65] with relation $U' = U - 2J_H$, and U, U', J_H are on-site Coulomb repulsions of the same and different orbitals and Hund's coupling, respectively.

We further express the tight-binding kernel as

$$H(\mathrm{k}) = \begin{bmatrix} H^x(\mathrm{k}) & H^{xz}(\mathrm{k}) \\ H^{xz}(\mathrm{k}) & H^z(\mathrm{k}) \end{bmatrix}, \tag{2}$$

in which $H^{x/z}(\mathrm{k})$ is the trilayer tight-binding matrix of $d_{x^2-y^2}/d_{z^2}$ orbital, and $H^{xz}(\mathrm{k})$ is the hybridization between them. They are expressed as

$$\begin{aligned} H^{x/z}_{11} &= H^{x/z}_{33} = \epsilon^{x/z,\mathrm{O}} + 2t^{x/z,\mathrm{O}}_{[1,0]}(\cos k_x + \cos k_y) + 4t^{x/z,\mathrm{O}}_{[1,1]} \cos k_x \cos k_y + 2t^{x/z,\mathrm{O}}_{[2,0]}(\cos 2k_x + \cos 2k_y), \\ H^{x/z}_{22} &= \epsilon^{x/z,\mathrm{I}} + 2t^{x/z,\mathrm{I}}_{[1,0]}(\cos k_x + \cos k_y) + 4t^{x/z,\mathrm{I}}_{[1,1]} \cos k_x \cos k_y + 2t^{x/z,\mathrm{I}}_{[2,0]}(\cos 2k_x + \cos 2k_y), \\ H^{x/z}_{12} &= H^{x/z}_{23} = t^{x/z,\mathrm{IO}}_{[0,0]} + 2t^{x/z,\mathrm{IO}}_{[1,0]}(\cos k_x + \cos k_y), \quad H^z_{13} = t^{z,\mathrm{OO}}_{[0,0]}, \\ H^{xz}_{11} &= H^{xz}_{33} = 2t^{xz,\mathrm{O}}_{[1,0]}(\cos k_x - \cos k_y) + 2t^{xz,\mathrm{O}}_{[2,0]}(\cos 2k_x - \cos 2k_y), \\ H^{xz}_{22} &= 2t^{xz,\mathrm{I}}_{[1,0]}(\cos k_x - \cos k_y) + 2t^{xz,\mathrm{I}}_{[2,0]}(\cos 2k_x - \cos 2k_y), \quad H^{xz}_{12} = H^{xz}_{23} = 2t^{xz,\mathrm{IO}}_{[1,0]}(\cos k_x - \cos k_y). \end{aligned} \tag{3}$$

We consider the hoppings up to the third-nearest neighbor in order to accurately describe the low-lying state of our DFT, which yields a total of 25 parameters listed in Table II. Some of the major hoppings are demonstrated in the schematic in Fig. 3(a). Here $t^{x,\mathrm{I}}_{[1,0]}$ denotes in-plane nearest-neighbor hopping of $d_{x^2-y^2}$ orbitals inside inner layer, and $t^{z,\mathrm{IO}}_{[0,0]}$ denotes perpendicular hopping of d_{z^2} orbital between inner and outer layers. According to the values in Table II, we find that most of the hoppings are enhanced comparably with respect to bilayer $La_3Ni_2O_7$. Practically, $t^x_{[1,0]}$ is enhanced from -0.483 to -0.521 (inner) or -0.511 (outer), and $t^{z,\mathrm{IO}}_{[0,0]}$ from -0.635 to -0.738 [11]. Such enhancement of hopping parameters

TABLE II. Tight-binding parameters of trilayer two-orbital model for $La_4Ni_3O_{10}$ under pressure. $t^{x/z}_{[i,j]}$ denotes the hopping term that is connected by [0,0]-[i, j] bond within $d_{x^2-y^2}/d_{z^2}$ orbital, while $t^{xz}_{[i,j]}$ denotes the hybridization between them, all in units of eV. The symmetrically equivalent terms are not shown for clarity.

Layer	i	j	$t^x_{[i,j]}$	$t^z_{[i,j]}$	$t^{xz}_{[i,j]}$
Inner	0	0	1.094	1.081	0
	1	0	−0.521	−0.168	0.298
	1	1	0.069	−0.018	0
	2	0	−0.076	−0.018	0.040
Outer	0	0	0.867	0.683	0
	1	0	−0.511	−0.143	0.274
	1	1	0.065	−0.015	0
	2	0	−0.074	−0.017	0.039
Inner-outer	0	0	0.035	−0.738	0
	1	0	0	0.033	−0.057
Outer-outer	0	0	0	−0.078	0

partially reflect a relative weaker correlation of trilayer than that of bilayer.

Based on the trilayer two-orbital model, we calculate the densities of $d_{x^2-y^2}$ and d_{z^2} orbitals, which are 0.62 and 0.54 for the inner layer, 0.55 and 0.63 for the outer layer, respectively. These correspond to an average $3d^{7.17}$ configuration, in exact agreement with previous analysis. According to the configuration, we roughly obtain the schematic depicted in Fig. 3(b). Here there have about two electrons on the d_{z^2} orbital forming a fully filled bonding state, while the nonbonding state is close to empty. The remaining two electrons reside on the $d_{x^2-y^2}$ orbital with the same spin alignment.

In Fig. 4, we further show the band structure and Fermi surface of the trilayer two-orbital model, which is in good agreement with our DFT results. The model is expressed under the primitive cell that contains only three Ni atoms, hence the flat band will be unfolded from the Γ to M point, as shown by the γ pocket in Fig. 4(b). The figure also reveals another three pockets α, β, β' with β, β' very close in each other. In general, the Fermi surface profile as well as the orbital weights are quite similar to that of the bilayer $La_3Ni_2O_7$ [11], as the γ point is uniquely characterized by the d_{z^2} orbital and α, β, β' pockets by mixing of d_{z^2} and $d_{x^2-y^2}$ orbitals. Finally, we note that the band structure shows a slight deviation from DFT at the X point under E_F, which is a compromise for a more accurate fitting of the Fermi surface during our modeling.

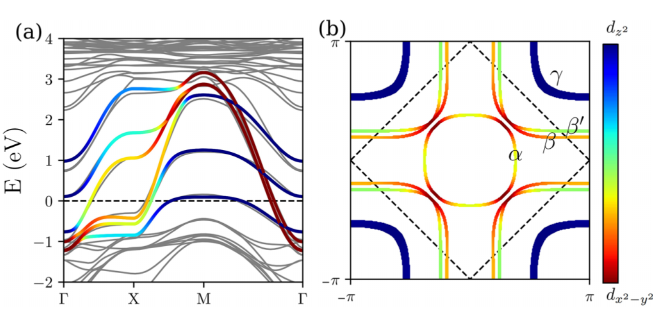

FIG. 4. (a) Band structure and (b) Fermi surface of trilayer two-orbital model. The color bar indicates the orbital weight of Ni-$d_{3z^2-r^2}$ and $d_{x^2-y^2}$. The grey lines in (a) are band structures from DFT (LDA, $U = 0$ eV). The diamond shape in (b) indicates the folded Brillouin zone.

To illustrate the bonding feature in $La_4Ni_3O_{10}$, we perform a rotation of the orbital basis under the trilayer symmetry, in which we define the new basis as

$$\Phi = (c_-, c_+, c)^T, \quad c_\pm = \frac{1}{\sqrt{2}}(d_1 \pm d_3), \quad c = d_2, \quad (4)$$

with d applied for both d_x and d_z operators. When along the nodal direction ($|k_x| = |k_y|$), the two e_g orbitals are well decoupled as the off-diagonal $H^{xz}(\mathrm{k}) = 0$ in Eq. (2). In this case, we can find that the nonbonding state is decisively characterized by the c_- state, namely, a sign-reversed superposition of states from two outer layers, while the bonding and antibonding states are associated with mixing of both c_+, c states [66]. For the most concerning bonding band of the Ni-d_{z^2} orbital, we can find that it is characterized by the positive superposition of c_+ and c, which corresponds to a more elongated Wannier wave function along the c axis.

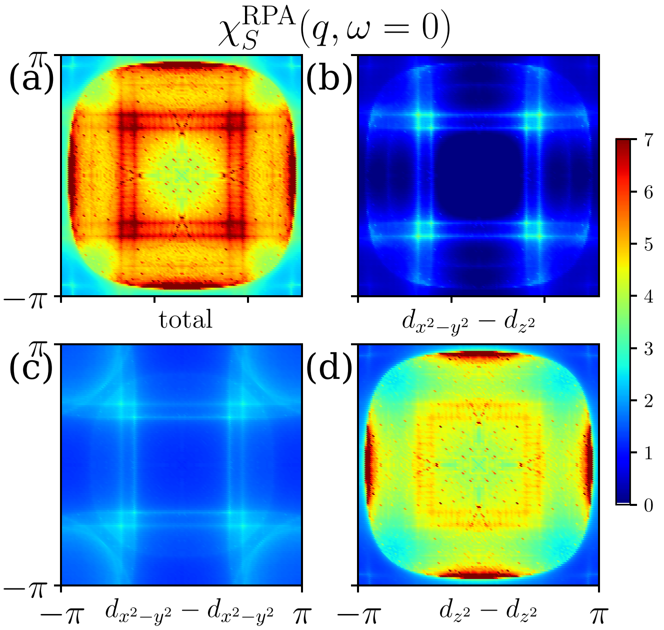

FIG. 5. RPA spin susceptibility $\chi_S^{st,\mathrm{RPA}}$ of trilayer two-orbital model. $U = 3.5$, $J = U/10$ are adopted in the calculation. (a) Orbital sum $\chi_S^{\mathrm{RPA}} = \sum_{st} \chi_S^{st,\mathrm{RPA}}$. (b)–(d) Orbital resolved $\chi_S^{st,\mathrm{RPA}}$. An amplify factor of 2 is used in (b), (c).

C. Spin susceptibility

The multi Fermi surface sheets of $La_4Ni_3O_{10}$ implies some possible magnetic instabilities that might be observed in experiments. In Fig. 5, we present the spin susceptibility of a trilayer two-orbital model at $\omega = 0$ under random phase approximation. The total orbital-summed $\chi_S^{\mathrm{RPA}} = \sum_{st} \chi_S^{st,\mathrm{RPA}}$ [Fig. 5(a)] shows a broad magnetic signal over the whole Brillouin zone, just like that in Ref. [62] as well as in a bilayer system [11,23,41]. Still, we can observe notable enhancement at some particular regimes reflecting fine nesting of the Fermi surface, especially at wave vector $\mathrm{q} = (\pm\frac{\pi}{2}, \pm\frac{\pi}{2})$.

From orbital-resolved $\chi_s^{st,\mathrm{RPA}}$ [Figs. 5(b)–5(d)], we find that it has a major d_{z^2} character, also the contribution from the $d_{x^2-y^2}$ orbital is non-negligible. Remarkably, the Fermi surface in Fig. 4(b) shows that such wave vectors are more associated with nesting within β, β' pockets which possess a quasi-1D feature and strong orbital mixing instead of α, γ pockets. This conjecture is also evidenced in χ_s^{RPA} by the appearance of a Moire pattern along these wave vectors, reflecting the quasidegeneracy of β, β' pockets. This highlights that the $d_{x^2-y^2}$ orbital is also important for the magnetic fluctuation of the ground state in $La_4Ni_3O_{10}$, despite it having a relatively weak correlation than d_{z^2} orbital [57]. Recently, the magnetic signal at this wave vector has been unambiguously revealed in a RIXS experiment for a bilayer system, indicating a corresponding double-stripe spin texture [67]. But according to the early experimental probe [63], the trilayer system, in fact, possesses an incommensurate magnetic wave vector $(0.62\pi, 0.62\pi)$, which is a bit deviated from the bilayer. We conjecture that such deviation is related to the strong interplay with a charge density wave or possibly charge fluctuation [68].

D. Sixteen-orbital model

In the previous trilayer two-orbital model, the oxygens are implicitly incorporated and the Ni-d orbital should be interpreted as a ligand-hold state in the sense of Sawatzky's picture [69,70]. In a dynamic mean-field theory (DMFT) study, the mapping from lattice to impurity problem requires explicit consideration of these conduction degree of freedoms [22,71]. Therefore, we further perform Wannier downfolding on both Ni-e_g and O-p orbitals. For each of the in-plane oxygens, we only pick one of the p_x/p_y orbitals that is elongated along its adjacent Ni site, as is usually done in a CuO_2 plane [71]. For apical oxygens, only p_z orbitals are selected. These yield a 16-orbital basis as demonstrated in the schematic in Fig. 6(c). In this basis, it is sufficient to consider merely 12 hopping parameters, which include the dominate nearest-neighbor dp, dd overlaps as listed in Table III. In this table, each hopping term is indicated by the orbital pairs which are connected by real-space vector [i,j,k], as can be located in the schematic. Note that the symmetrically equivalent terms are not shown for clarity. The site energies of these orbitals are also presented in the last two panels. The resulting band structure and Fermi surface are shown in Figs. 6(a) and 6(b), which are all in good agreement with our DFT results. The band structure covers an energy range of $-9 \sim 3$ eV, with strong split into two parts. We find there appear two flat bands in the lower part, which are originated from two dangling p_z' orbitals with strong coupling to apical d_{z^2} orbitals. The huge band split indicates a significantly large energy scale of dp hybridization, from which the effective direct dd couplings emerge, as illustrated in our trilayer two-orbital model. This model will be important for further study of strong correlation effects and superexchange couplings.

According to the table, the site-energy differences within the NiO_2 plane are calculated as $\epsilon_{x_2} - \epsilon_{px_2} = 3.42\,\mathrm{eV}$ and $\epsilon_{x_1} - \epsilon_{px_1} = 3.68\,\mathrm{eV}$, respectively, for inner and outer layers. Along the apical direction, the energy differences are $\epsilon_{z_2} - \epsilon_{p_z} = 3.47$ eV or $\epsilon_{z_1} - \epsilon_{p_z} = 3.14$ eV. Compared with bilayer, these magnitudes are quite similar, and both suggest a relative smaller energy difference between d_{z^2} and apical p_z orbitals than that of the cuprate counterpart. This implies that $La_4Ni_3O_{10}$ should also lie in the charge-transfer picture [22], and would favor a strong interlayer superexchange coupling [72,73]. However, for trilayer, the microscopic superexchange

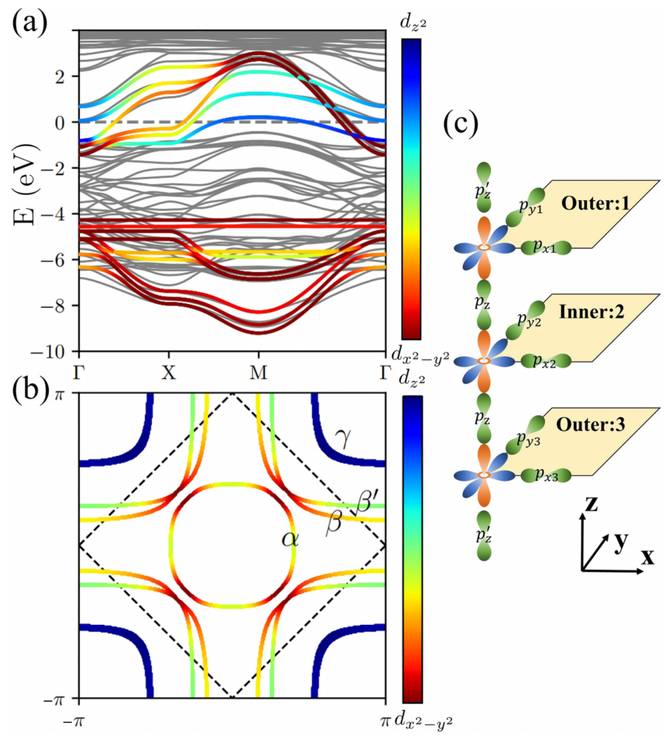

FIG. 6. (a) Band structure and (b) Fermi surface of 16-orbital model. The color bar indicates the orbital weight of Ni-$d_{3z^2-r^2}$ and $d_{x^2-y^2}$ orbitals. The grey lines in (a) are band structures from DFT (LDA, $U = 0$ eV). The diamond shape in (b) indicates the folded Brillouin zone. (c) Schematic of 16 orbitals for 16-orbital model.

TABLE III. Tight-binding parameters of 16-orbital model for $La_4Ni_3O_{10}$ under pressure, in unit of eV. The corresponding orbitals are displayed in Fig. 6(b). The symmetrically equivalent terms are not shown for clarity.

Hopping	$d_{z_3} - p_z$ $[0,0,\frac{1}{2}]$	$d_{z_2} - p_z$ $[0,0,\frac{1}{2}]$	$d_{x_2} - p_{x_2}$ $[\frac{1}{2},0,0]$	$d_{x_1} - p_{x_1}$ $[\frac{1}{2},0,0]$
t	1.911	1.523	1.681	1.676
Hopping	$d_{z_1} - p_z'$ $[0,0,\frac{1}{2}]$	$d_{z_2} - p_{x_2}$ $[\frac{1}{2},0,0]$	$d_{z_1} - p_{x_1}$ $[\frac{1}{2},0,0]$	$p_{x_1} - p_{y_1}$ $[\frac{1}{2},\frac{1}{2},0]$
t	1.591	−0.938	−0.887	0.604
Hopping	$p_{x_2} - p_{y_2}$ $[\frac{1}{2},\frac{1}{2},0]$	$p_z - p_{x_1}$ $[\frac{1}{2},0,\frac{1}{2}]$	$p_z - p_{x_2}$ $[\frac{1}{2},0,\frac{1}{2}]$	$p_z' - p_{x_1}$ $[\frac{1}{2},0,-\frac{1}{2}]$
t	0.553	0.597	0.577	−0.465
Site	ϵ_{x_1}	ϵ_{z_1}	ϵ_{x_2}	ϵ_{z_2}
Energy	−1.431	−1.354	−1.075	−1.027
Site	ϵ_{px_1}	ϵ_{px_2}	ϵ_{p_z}	$\epsilon_{p_z'}$
Energy	−5.109	−4.757	−4.494	−4.149

couplings is supposed to be more complicated as there involve at least three d_{z^2} and p_z orbitals. For example, the superexchange process of $d_{z^2} - p_z - d_{z^2}$ between two adjacent layers, which is believed to be dominant in the bilayer system [73], would be depressed in trilayer due to interference from other d_{z^2} and p_z along the c axis, and we believe that might be the reason for a much lower transition temperature in $La_4Ni_3O_{10}$. Also, such speculation is in line with the fundamental concept that correlation is depressed in higher dimensions.

V. DISCUSSION

The microscopic charge transfer processes as well as the associating dual effect reflect two impulses from pressure. For the first one, the charge transfer from Ni-e_g to t_{2g} under pressure can be directly attributed to the octahedral tilting as illustrated in Sec. II. Meanwhile, a lattice that possesses higher symmetry is generally preferred by a uniform pressure, which corresponds to the $I4/mmm$ phase in the case of the RP series. This can be simply understood from the definition of enthalpy $H = U + PV$, which shows that pressure would push the lattice to a higher energy state, where the symmetry unbreaking state is preferred. For the second one, the partial charge transfer from Ni-d to La ions essentially reflects an urge from lattice collapse, which is strongly reminiscent of the lanthanide contraction effect [74]. In the lanthanide series, the removal of correlated $4f$ electrons under pressure (or lowering temperature) causes a decrease of screening from the nucleus charge, so the outer valence electrons are sucked in closer to the nucleus, further causing a decrease in ion radius [74]. More importantly, the partial filling of these correlated orbitals gives rise to valence fluctuation phenomenon. In RP series compounds, an analogous dynamic mechanism should be applied, which suggests a likewise enhanced valence fluctuation under pressure. In this sense, the superconductivity can be interpreted as an unexpected outcome of valence fluctuation within Ni-e_g orbitals.

Based on the above analysis, we further elucidate the dynamic mechanism of electronic reconstructions under pressure. As we gradually apply pressure onto the lattice, both effects happen simultaneously, jointly leading to the upward shift of the Ni-e_g spectrum. Note that their respective contributions should be different, and according to our results, the second effect has the dominate role. However, the first effect might also be indispensable, as there is a conjecture that the straightening of the apical Ni-O-Ni bond angle can significantly enhance the perpendicular superexchange $J_\perp$, which is crucial for the occurrence of superconductivity. Once the pressure is high enough for such bond angle to reach formal 180°, it corresponds to a structure transition. For even higher pressure, a new situation appears. In this stage, the oxygens within the NiO_2 plane start to move along the c axis, leading to a separation of the basal oxygens and Ni planes, but it maintains the invariance of a $I4/mmm$ structure [49]. This structure variation is related to a further lattice collapse along the a/b axis, while the collapse along the c axis has largely depleted in the early stage. In this stage, it can be expected that there should be a charge transfer from the Ni-d_{z^2} to $d_{x^2-y^2}$ orbital, further pushing the Ni-d_{z^2} spectrum towards higher energy. Overall, we believe our exposition of the dynamic mechanism of electronic reconstructions is particularly helpful for theoretical understanding of electronic properties in the RP series, which can inspire various further theoretical investigations on various aspects, such as valence fluctuation, superexchanges, correlation renormalization effect [42,75], orbital selective property [11,39,67,76,77], strange metal behavior [7,78], and the interplay with spin/charge density wave fluctuations [63]. Moreover, it sheds light on experimental exploration of superconductors under low pressure via chemical substitute.

Finally, regarding the layer dependence, our investigations on electronic properties of $La_4Ni_3O_{10}$ have strongly recommended a similar superconducting mechanism among the RP series, in which the increase of layer seems to trivially play a negative role. We tend to believe the suppression of T_c is largely related to the decrease of correlation, while the latter can be understood in such a way: As the bonding state of the d_{z^2} orbital always has a Wannier function that is elongated along the c axis all over the layers, the increase of layer indicates a more extended ground-state wave function, which in turn weakens the correlation. If so, it would be unsurprising that superconductivity is fully depressed in quadlayer $La_5Ni_4O_{13}$ even which possesses an alike Fermi surface profile [50]. Nevertheless, such an experimental observation is still of significance. All these features highlight that the RP series is a perfect platform for theoretical understanding of the unconventional superconducting mechanism. Also, the role of the even-odd effect, which governs the excitation gap in local spin-$\frac{N}{2}$ chain, remains clear in the series [59,79,80].

VI. SUMMARY

In summary, we performed comprehensive DFT calculations on RP series $La_4Ni_3O_{10}$ for both AP $P2_1/a$ and HP $I4/mmm$ phases, with $U = 0, 3.5$ eV. Our results clearly reveal the characteristic upward shift of the Ni-d_{z^2} bonding band under pressure, suggesting a crucial link to the superconductivity in the RP series. Our analysis of electronic spectra as well as orbital occupancies indicate a charge transfer of $3d^{8.36} \rightarrow 3d^{8.14}$ under pressure, specifically, $2.44 \rightarrow 2.14$ for Ni-e_g and $5.92 \rightarrow 6.0$ for Ni-t_{2g} sectors. These trends indicate a critical dual effect of pressure, in which pressure, on one hand, promotes a charge redistribution within Ni-e_g and t_{2g} sectors. On the other hand, pressure drives a partial charge transfer from Ni to La ions. On this basis, in the discussion, we fully unveil the dynamic mechanism of electronic reconstructions under pressure, which sheds light on theoretical understanding of electronic correlations and superconductivity, as well as on experimental exploration of superconductors with lower pressure.

Based on our DFT results, we proposed a trilayer two-orbital model by performing Wannier downfolding on Ni-e_g orbitals. This model reveals four Fermi pockets $\alpha, \beta, \beta', \gamma$, which is very close to that of $La_4Ni_3O_{10}$, suggesting a similar superconducting mechanism in the RP series. Also, our calculated RPA spin susceptibility suggests that $d_{x^2-y^2}$ orbitals should also be important for the magnetic fluctuation in RP series.

To gain insights into the charge-transfer property within the Zaanen-Sawatzky-Allen (ZSA) scheme, we further proposed a high energy 16-orbital model based on Wannier downfolding on both Ni-e_g and O-p orbitals. The model also well reproduces the low-lying band structure, with merely 12 nearest-neighbor dd, dp hoppings. The site energies of the model show that the energy differences between Ni-d and O-p orbitals are close to that in bilayer, which are 3.42 and 3.68 eV, respectively, for inner and outer layers between $d_{x^2-y^2} - p_x/p_y$, and 3.47, 3.14 eV for apical $d_{z^2} - p_z$ orbitals. This implies that $La_4Ni_3O_{10}$ also lies in the charge-transfer picture within ZAS scheme. In short, the 16-orbital model as well as the trilayer two-orbital model are important for future study of strong correlation effects and unconventional pairing symmetry.

Note added. Recently, we noticed several works [81–87] showing consistency with our results.

ACKNOWLEDGMENTS

We are grateful to Q.-H. Wang, G.-M. Zhang, and X. Hu for fruitful discussions. Work at Sun Yat-Sen University was supported by the National Key Research and Development Program of China (Grants No. 2022YFA1402802, No. 2018YFA0306001, and No. 2023YFA1406500), the National Natural Science Foundation of China (Grants No. 92165204, No. 12174454, No. 11974432, and No. 12274472), the Guangdong Basic and Applied Basic Research Foundation (Grants No. 2022A1515011618 and No. 2024B1515020040), Guangzhou Basic and Applied Basic Research Funds (Grant No. 2024A04J6417), Guangdong Provincial Key Laboratory of Magnetoelectric Physics and Devices (Grant No. 2022B1212010008), and Shenzhen International Quantum Academy (Grant No. SIQA202102).

[1] D. Li, K. Lee, B. Y. Wang, M. Osada, S. Crossley, H. R. Lee, Y. Cui, Y. Hikita, and H. Y. Hwang, Superconductivity in an infinite-layer nickelate, Nature (London) **572**, 624 (2019).

[2] S. Zeng, C. Li, L. E. Chow, Y. Cao, Z. Zhang, C. S. Tang, X. Yin, Z. S. Lim, J. Hu, P. Yang, and A. Ariando, Superconductivity in infinite-layer nickelate $La_{1-x}Ca_xNiO_2$ thin films, Sci. Adv. **8**, eabl9927 (2022).

[3] M. Osada, B. Y. Wang, B. H. Goodge, K. Lee, H. Yoon, K. Sakuma, D. Li, M. Miura, L. F. Kourkoutis, and H. Y. Hwang, A superconducting praseodymium nickelate with infinite layer structure, Nano Lett. **20**, 5735 (2020).

[4] H. Sun, M. Huo, X. Hu, J. Li, Z. Liu, Y. Han, L. Tang, Z. Mao, P. Yang, B. Wang, J. Cheng, D.-X. Yao, G.-M. Zhang, and M. Wang, Signatures of superconductivity near 80 K in a nickelate under high pressure, Nature (London) **621**, 493 (2023).

[5] G. Wang, N. N. Wang, X. L. Shen, J. Hou, L. Ma, L. F. Shi, Z. A. Ren, Y. D. Gu, H. M. Ma, P. T. Yang, Z. Y. Liu, H. Z. Guo, J. P. Sun, G. M. Zhang, S. Calder, J.-Q. Yan, B. S. Wang, Y. Uwatoko, and J.-G. Cheng, Pressure-induced superconductivity in polycrystalline $La_3Ni_2O_{7-\delta}$, Phys. Rev. X **14**, 011040 (2024).

[6] J. Hou, P.-T. Yang, Z.-Y. Liu, J.-Y. Li, P.-F. Shan, L. Ma, G. Wang, N.-N. Wang, H.-Z. Guo, J.-P. Sun, Y. Uwatoko, M. Wang, G.-M. Zhang, B.-S. Wang, and J.-G. Cheng, Emergence of high-temperature superconducting phase in pressurized $La_3Ni_2O_7$ crystals, Chin. Phys. Lett. **40**, 117302 (2023).

[7] Y. Zhu, E. Zhang, B. Pan, X. Chen, D. Peng, L. Chen, H. Ren, F. Liu, N. Li, Z. Xing, J. Han, J. Wang, D. Jia, H. Wo, Y. Gu, Y. Gu, L. Ji, W. Wang, H. Gou, Y. Shen *et al.*, Superconductivity in trilayer nickelate $La_4Ni_3O_{10}$ single crystals, arXiv:2311.07353.

[8] Y. Zhou, J. Guo, S. Cai, H. Sun, P. Wang, J. Zhao, J. Han, X. Chen, Q. Wu, Y. Ding, M. Wang, T. Xiang, H. Kwang Mao, and L. Sun, Evidence of filamentary superconductivity in pressurized $La_3Ni_2O_7$ single crystals, arXiv:2311.12361.

[9] M. Zhang, C. Pei, X. Du, Y. Cao, Q. Wang, J. Wu, Y. Li, Y. Zhao, C. Li, W. Cao, S. Zhu, Q. Zhang, N. Yu, P. Cheng, J. Zhao, Y. Chen, H. Guo, L. Yang, and Y. Qi, Superconductivity in trilayer nickelate $La_4Ni_3O_{10}$ under pressure, arXiv:2311.07423.

[10] Q. Li, Y.-J. Zhang, Z.-N. Xiang, Y. Zhang, X. Zhu, and H.-H. Wen, Signature of superconductivity in pressurized $La_4Ni_3O_{10}$, Chin. Phys. Lett. **41**, 017401 (2024).

[11] Z. Luo, X. Hu, M. Wang, W. Wú, and D.-X. Yao, Bilayer two-orbital model of $La_3Ni_2O_7$ under pressure, Phys. Rev. Lett. **131**, 126001 (2023).

[12] Z. Luo, B. Lv, M. Wang, W. Wú, and D.-X. Yao, High-T_C superconductivity in $La_3Ni_2O_7$ based on the bilayer two-orbital *t-J* model, arXiv:2308.16564.

[13] C. C. Tam, J. Choi, X. Ding, S. Agrestini, A. Nag, M. Wu, B. Huang, H. Luo, P. Gao, M. Garcia-Fernandez, L. Qiao, and K. Zhou, Charge density waves in infinite-layer $NdNiO_2$ nickelates, Nat. Mater. **21**, 1116 (2022).

[14] Z. Liu, Z. Ren, W. Zhu, Z. Wang, and J. Yang, Electronic and magnetic structure of infinite-layer $NdNiO_2$: Trace of antiferromagnetic metal, npj Quantum Mater. **5**, 31 (2020).

[15] Z. Liu, H. Sun, M. Huo, X. Ma, Y. Ji, E. Yi, L. Li, H. Liu, J. Yu, Z. Zhang, Z. Chen, F. Liang, H. Dong, H. Guo, D. Zhong, B. Shen, S. Li, and M. Wang, Evidence for charge and spin density waves in single crystals of $La_3Ni_2O_7$ and $La_3Ni_2O_6$, Sci. China Phys. Mech. Astron. **66**, 217411 (2023).

[16] L.-H. Hu and C. Wu, Two-band model for magnetism and superconductivity in nickelates, Phys. Rev. Res. **1**, 032046(R) (2019).

[17] Y. Zhang, L.-F. Lin, A. Moreo, T. A. Maier, and E. Dagotto, Electronic structure, magnetic correlations, and superconducting pairing in the reduced Ruddlesden-Popper bilayer $La_3Ni_2O_6$ under pressure: Different role of $d_{3z^2-r^2}$ orbital compared with $La_3Ni_2O_7$, Phys. Rev. B **109**, 045151 (2024).

[18] Y. Shen, M. Qin, and G.-M. Zhang, Effective bi-layer model Hamiltonian and density-matrix renormalization group study for the high-T_c superconductivity in $La_3Ni_2O_7$ under high pressure, Chin. Phys. Lett. **40**, 127401 (2023).

[19] D. X. Yao and E. W. Carlson, Spin-wave dispersion in half-doped $La_{3/2}Sr_{1/2}NiO_4$, Phys. Rev. B **75**, 012414 (2007).

[20] S. Ryee, H. Yoon, T. J. Kim, M. Y. Jeong, and M. J. Han, Induced magnetic two-dimensionality by hole doping in the

superconducting infinite-layer nickelate $Nd_{1-x}Sr_xNiO_2$, Phys. Rev. B **101**, 064513 (2020).

[21] Q. Qin and Y.-F. Yang, High-T_c superconductivity by mobilizing local spin singlets and possible route to higher T_c in pressurized $La_3Ni_2O_7$, Phys. Rev. B **108**, L140504 (2023).

[22] W. Wú, Z. Luo, D.-X. Yao, and M. Wang, Superexchange and charge transfer in the nickelate superconductor $La_3Ni_2O_7$ under pressure, Sci. China Phys. Mech. Astron. **67**, 117402 (2024).

[23] S. Botzel, F. Lechermann, J. Gondolf, and I. M. Eremin, Theory of magnetic excitations in multilayer nickelate superconductor $La_3Ni_2O_7$, Phys. Rev. B **109**, L180502 (2024).

[24] Y. Nomura, M. Hirayama, T. Tadano, Y. Yoshimoto, K. Nakamura, and R. Arita, Formation of a two-dimensional single-component correlated electron system and band engineering in the nickelate superconductor $NdNiO_2$, Phys. Rev. B **100**, 205138 (2019).

[25] A. S. Botana and M. R. Norman, Similarities and differences between $LaNiO_2$ and $CaCuO_2$ and implications for superconductivity, Phys. Rev. X **10**, 011024 (2020).

[26] M. Jiang, M. Berciu, and G. A. Sawatzky, Critical nature of the Ni spin state in doped $NdNiO_2$, Phys. Rev. Lett. **124**, 207004 (2020).

[27] G.-M. Zhang, Y.-F. Yang, and F.-C. Zhang, Self-doped Mott insulator for parent compounds of nickelate superconductors, Phys. Rev. B **101**, 020501(R) (2020).

[28] Y.-H. Zhang and A. Vishwanath, Type-II $t-J$ model in superconducting nickelate $Nd_{1-x}Sr_xNiO_2$, Phys. Rev. Res. **2**, 023112 (2020).

[29] P. Werner and S. Hoshino, Nickelate superconductors: Multiorbital nature and spin freezing, Phys. Rev. B **101**, 041104(R) (2020).

[30] F. Bernardini, V. Olevano, and A. Cano, Magnetic penetration depth and T_c in superconducting nickelates, Phys. Rev. Res. **2**, 013219 (2020).

[31] M. Hepting, D. Li, C. J. Jia, H. Lu, E. Paris, Y. Tseng, X. Feng, M. Osada, E. Been, Y. Hikita, Y. D. Chuang, Z. Hussain, K. J. Zhou, A. Nag, M. Garcia-Fernandez, M. Rossi, H. Y. Huang, D. J. Huang, Z. X. Shen, T. Schmitt *et al.*, Electronic structure of the parent compound of superconducting infinite-layer nickelates, Nat. Mater. **19**, 381 (2020).

[32] Y. Gu, S. Zhu, X. Wang, J. Hu, and H. Chen, A substantial hybridization between correlated Ni-d orbital and itinerant electrons in infinite-layer nickelates, Commun. Phys. **3**, 84 (2020).

[33] J. Chang, J. Zhao, and Y. Ding, Hund-Heisenberg model in superconducting infinite-layer nickelates, Eur. Phys. J. B **93**, 220 (2020).

[34] M. Kitatani, L. Si, O. Janson, R. Arita, Z. Zhong, and K. Held, Nickelate superconductors—a renaissance of the one-band Hubbard model, npj Quantum Mater. **5**, 59 (2020).

[35] G. Krieger, L. Martinelli, S. Zeng, L. E. Chow, K. Kummer, R. Arpaia, M. Moretti Sala, N. B. Brookes, A. Ariando, N. Viart, M. Salluzzo, G. Ghiringhelli, and D. Preziosi, Charge and spin order dichotomy in $NdNiO_2$ driven by the capping layer, Phys. Rev. Lett. **129**, 027002 (2022).

[36] X. Wu, D. Di Sante, T. Schwemmer, W. Hanke, H. Y. Hwang, S. Raghu, and R. Thomale, Robust $d_{x^2-y^2}$-wave superconductivity of infinite-layer nickelates, Phys. Rev. B **101**, 060504(R) (2020).

[37] Z. Luo, D.-X. Yao, and W. Wú, Superconductivity in the two-orbital Hubbard model of infinite-layer nickelates, arXiv:2310.12250.

[38] Z. Fan, J.-F. Zhang, B. Zhan, D. Lv, X.-Y. Jiang, B. Normand, and T. Xiang, Superconductivity in nickelate and cuprate superconductors with strong bilayer coupling, arXiv:2312.17064.

[39] D. A. Shilenko and I. V. Leonov, Correlated electronic structure, orbital-selective behavior, and magnetic correlations in double-layer $La_3Ni_2O_7$ under pressure, Phys. Rev. B **108**, 125105 (2023).

[40] Q.-G. Yang, D. Wang, and Q.-H. Wang, Possible $s_\pm$-wave superconductivity in $La_3Ni_2O_7$, Phys. Rev. B **108**, L140505 (2023).

[41] Y. Gu, C. Le, Z. Yang, X. Wu, and J. Hu, Effective model and pairing tendency in bilayer Ni-based superconductor $La_3Ni_2O_7$, arXiv:2306.07275.

[42] J. Yang, H. Sun, X. Hu, Y. Xie, T. Miao, H. Luo, H. Chen, B. Liang, W. Zhu, G. Qu, C.-Q. Chen, M. Huo, Y. Huang, S. Zhang, F. Zhang, F. Yang, Z. Wang, Q. Peng, H. Mao, G. Liu *et al.*, Orbital-dependent electron correlation in double-layer nickelate $La_3Ni_2O_7$, Nat. Commun. **15**, 4373 (2024).

[43] M. Zhang, C. Pei, Q. Wang, Y. Zhao, C. Li, W. Cao, S. Zhu, J. Wu, and Y. Qi, Effects of pressure and doping on Ruddlesden-Popper phases $La_{n+1}Ni_nO_{3n+1}$, J. Mater. Sci. Technol. **185**, 147 (2024).

[44] N. Yuan, A. Elghandour, J. Arneth, K. Dey, and R. Klingeler, High-pressure crystal growth and investigation of the metal-to-metal transition of Ruddlesden-Popper trilayer nickelates $La_4Ni_3O_{10}$, J. Cryst. Growth **627**, 127511 (2024).

[45] Q. Li, C. He, J. Si, X. Zhu, Y. Zhang, and H.-H. Wen, Absence of superconductivity in bulk $Nd_{1-x}Sr_xNiO_2$, Commun. Mater. **1**, 16 (2020).

[46] R. Jiang, J. Hou, Z. Fan, Z.-J. Lang, and W. Ku, Pressure driven fractionalization of ionic spins results in cupratelike high-T_c superconductivity in $La_3Ni_2O_7$, Phys. Rev. Lett. **132**, 126503 (2024).

[47] J. Li, C.-Q. Chen, C. Huang, Y. Han, M. Huo, X. Huang, P. Ma, Z. Qiu, J. Chen, X. Hu, L. Chen, T. Xie, B. Shen, H. Sun, D.-X. Yao, and M. Wang, Structural transition, electric transport, and electronic structures in the compressed trilayer nickelate $La_4Ni_3O_{10}$, Sci. China Phys. Mech. Astron. **67**, 117403 (2024).

[48] L. Wang, Y. Li, S. Xie, F. Liu, H. Sun, C. Huang, Y. Gao, T. Nakagawa, B. Fu, B. Dong, Z. Cao, R. Yu, S. I. Kawaguchi, H. Kadobayashi, M. Wang, C. Jin, H. kwang Mao, and H. Liu, Structure responsible for the superconducting state in $La_3Ni_2O_7$ at high pressure and low temperature conditions, arXiv:2311.09186.

[49] B. Geisler, J. J. Hamlin, G. R. Stewart, R. G. Hennig, and P. J. Hirschfeld, Structural transitions, octahedral rotations, and electronic properties of $A_3Ni_2O_7$ rare-earth nickelates under high pressure, npj Quantum Mater. **9**, 38 (2024).

[50] M.-C. Jung, J. Kapeghian, C. Hanson, B. Pamuk, and A. S. Botana, Electronic structure of higher-order Ruddlesden-Popper nickelates, Phys. Rev. B **105**, 085150 (2022).

[51] G. Kresse and J. Furthmuller, Efficiency of ab-initio total energy calculations for metals and semiconductors using a plane-wave basis set, Comput. Mater. Sci. **6**, 15 (1996).

[52] G. Kresse and J. Furthmuller, Efficient iterative schemes for *ab initio* total-energy calculations using a plane-wave basis set, Phys. Rev. B **54**, 11169 (1996).
[53] P. E. Blochl, Projector augmented-wave method, Phys. Rev. B **50**, 17953 (1994).
[54] G. Kresse and D. Joubert, From ultrasoft pseudopotentials to the projector augmented-wave method, Phys. Rev. B **59**, 1758 (1999).
[55] W. Kohn and L. J. Sham, Self-consistent equations including exchange and correlation effects, Phys. Rev. **140**, A1133 (1965).
[56] A. A. Mostofi, J. R. Yates, Y.-S. Lee, I. Souza, D. Vanderbilt, and N. Marzari, wannier90: A tool for obtaining maximally-localised Wannier functions, Comput. Phys. Commun. **178**, 685 (2008).
[57] H. Li, X. Zhou, T. Nummy, J. Zhang, V. Pardo, W. E. Pickett, J. F. Mitchell, and D. S. Dessau, Fermiology and electron dynamics of trilayer nickelate $La_4Ni_3O_{10}$, Nat. Commun. **8**, 704 (2017).
[58] V. Christiansson, F. Petocchi, and P. Werner, Correlated electronic structure of $La_3Ni_2O_7$ under pressure, Phys. Rev. Lett. **131**, 206501 (2023).
[59] H. Sakakibara, M. Ochi, H. Nagata, Y. Ueki, H. Sakurai, R. Matsumoto, K. Terashima, K. Hirose, H. Ohta, M. Kato, Y. Takano, and K. Kuroki, Theoretical analysis on the possibility of superconductivity in the trilayer Ruddlesden-Popper nickelate $La_4Ni_3O_{10}$ under pressure and its experimental examination: Comparison with $La_3Ni_2O_7$, Phys. Rev. B **109**, 144511 (2024).
[60] Y. Kamihara, H. Hiramatsu, M. Hirano, R. Kawamura, H. Yanagi, T. Kamiya, and H. Hosono, Iron-based layered superconductor: LaOFeP, J. Am. Chem. Soc. **128**, 10012 (2006).
[61] S. Lebègue, Electronic structure and properties of the Fermi surface of the superconductor LaOFeP, Phys. Rev. B **75**, 035110 (2007).
[62] I. V. Leonov, Electronic structure and magnetic correlations in trilayer nickelate superconductor $La_4Ni_3O_{10}$ under pressure, Phys. Rev. B **109**, 235123 (2024).
[63] J. Zhang, D. Phelan, A. S. Botana, Y. S. Chen, H. Zheng, M. Krogstad, S. G. Wang, Y. Qiu, J. A. Rodriguez-Rivera, R. Osborn, S. Rosenkranz, M. R. Norman, and J. F. Mitchell, Intertwined density waves in a metallic nickelate, Nat. Commun. **11**, 6003 (2020).
[64] M. R. Norman, A. S. Botana, J. Karp, A. Hampel, H. LaBollita, A. J. Millis, G. Fabbris, Y. Shen, and M. P. M. Dean, Orbital polarization, charge transfer, and fluorescence in reduced-valence nickelates, Phys. Rev. B **107**, 165124 (2023).
[65] A. Georges, L. de' Medici, and J. Mravlje, Strong correlations from Hund's coupling, Annu. Rev. Condens. Matter Phys. **4**, 137 (2013).
[66] W. Sun, Y. Li, X. Cai, J. Yang, W. Guo, Z. Gu, Y. Zhu, and Y. Nie, Electronic and transport properties in Ruddlesden-Popper neodymium nickelates $Nd_{n+1}Ni_nO_{3n+1}$ ($n = 1 - 5$), Phys. Rev. B **104**, 184518 (2021).
[67] X. Chen, J. Choi, Z. Jiang, J. Mei, K. Jiang, J. Li, S. Agrestini, M. Garcia-Fernandez, X. Huang, H. Sun, D. Shen, M. Wang, J. Hu, Y. Lu, K.-J. Zhou, and D. Feng, Electronic and magnetic excitations in $La_3Ni_2O_7$, arXiv:2401.12657.
[68] Y. T. Tam, D. X. Yao, and W. Ku, Itinerancy-enhanced quantum fluctuation of magnetic moments in iron-based superconductors, Phys. Rev. Lett. **115**, 117001 (2015).
[69] J. Zaanen, G. A. Sawatzky, and J. W. Allen, Band gaps and electronic structure of transition-metal compounds, Phys. Rev. Lett. **55**, 418 (1985).
[70] F. C. Zhang and T. M. Rice, Effective Hamiltonian for the superconducting Cu oxides, Phys. Rev. B **37**, 3759 (1988).
[71] N. Kowalski, S. S. Dash, P. Semon, D. Senechal, and A. M. Tremblay, Oxygen hole content, charge-transfer gap, covalency, and cuprate superconductivity, Proc. Natl. Acad. Sci. USA **118**, e2106476118 (2021).
[72] E. Been, W.-S. Lee, H. Y. Hwang, Y. Cui, J. Zaanen, T. Devereaux, B. Moritz, and C. Jia, Electronic structure trends across the rare-earth series in superconducting infinite-layer nickelates, Phys. Rev. X **11**, 011050 (2021).
[73] C. Lu, Z. Pan, F. Yang, and C. Wu, Interplay of two E_g orbitals in superconducting $La_3Ni_2O_7$ under pressure, arXiv:2310.02915.
[74] J. M. Lawrence, P. S. Riseborough, and R. D. Parks, Valence fluctuation phenomena, Rep. Prog. Phys. **44**, 1 (1981).
[75] Y.-H. Tian, Y. Chen, J.-M. Wang, R.-Q. He, and Z.-Y. Lu, Correlation effects and concomitant two-orbital $s_\pm$-wave superconductivity in $La_3Ni_2O_7$ under high pressure, Phys. Rev. B **109**, 165154 (2024).
[76] Y. Zhang, L.-F. Lin, A. Moreo, and E. Dagotto, Electronic structure, dimer physics, orbital-selective behavior, and magnetic tendencies in the bilayer nickelate superconductor $La_3Ni_2O_7$ under pressure, Phys. Rev. B **108**, L180510 (2023).
[77] Y.-F. Yang, G.-M. Zhang, and F.-C. Zhang, Interlayer valence bonds and two-component theory for high-T_c superconductivity of $La_3Ni_2O_7$ under pressure, Phys. Rev. B **108**, L201108 (2023).
[78] Y. Zhang, D. Su, Y. Huang, Z. Shan, H. Sun, M. Huo, K. Ye, J. Zhang, Z. Yang, Y. Xu, Y. Su, R. Li, M. Smidman, M. Wang, L. Jiao, and H. Yuan, High-temperature superconductivity with zero resistance and strange-metal behaviour in $La_3Ni_2O_{7-\delta}$, Nat. Phys. (2024), doi:10.1038/s41567-024-02515-y.
[79] E. Dagotto and T. M. Rice, Surprises on the way from one- to two-dimensional quantum magnets: The ladder materials, Science **271**, 618 (1996).
[80] J.-Q. Cheng, J. Li, Z. Xiong, H.-Q. Wu, A. W. Sandvik, and D.-X. Yao, Fractional and composite excitations of antiferromagnetic quantum spin trimer chains, npj Quantum Mater. **7**, 3 (2022).
[81] J.-X. Wang, Z. Ouyang, R.-Q. He, and Z.-Y. Lu, Non-Fermi liquid and Hund correlation in $La_4Ni_3O_{10}$ under high pressure, Phys. Rev. B **109**, 165140 (2024).
[82] Y. Zhang, L.-F. Lin, A. Moreo, T. A. Maier, and E. Dagotto, Prediction of $s^\pm$-wave superconductivity enhanced by electronic doping in trilayer nickelates $La_4Ni_3O_{10}$ under pressure, arXiv:2402.05285.
[83] Q.-G. Yang, K.-Y. Jiang, D. Wang, H.-Y. Lu, and Q.-H. Wang, Effective model and $s_\pm$-wave superconductivity in trilayer nickelate $La_4Ni_3O_{10}$, arXiv:2402.05447.
[84] C. Lu, Z. Pan, F. Yang, and C. Wu, Superconductivity in $La_4Ni_3O_{10}$ under pressure, arXiv:2402.06450.
[85] H. LaBollita, J. Kapeghian, M. R. Norman, and A. S. Botana, Electronic structure and magnetic tendencies

of trilayer $La_4Ni_3O_{10}$ under pressure: Structural transition, molecular orbitals, and layer differentiation, arXiv:2402.05085.

[86] P.-F. Tian, H.-T. Ma, X. Ming, X.-J. Zheng, and H. Li, Effective model and electron correlations in trilayer nickelate superconductor $La_4Ni_3O_{10}$, J. Phys.: Condens. Matter **36**, 355602 (2024).

[87] M. Zhang, H. Sun, Y.-B. Liu, Q. Liu, W.-Q. Chen, and F. Yang, The $s^{\pm}$-wave superconductivity in the pressurized $La_4Ni_3O_{10}$, arXiv:2402.07902.